Table of Contents

List of Figures

Abstract

A computer model is described that combines concepts from the fields of acoustics, linear system theory and digital signal processing to simulate an acoustic sensor navigation system using time-of-flight ranging. By separating the transmitter/receiver into separate components and assuming mirror-like reflectors, closed-form solutions for the reflections from corners, edges and walls are determined as a function of transducer size, location and orientation. A floor plan consisting of corners, walls and edges is efficiently encoded to indicate which of these elements contribute to a particular pulse-echo response. Sonar maps produced by transducers having different resonant frequencies and transmitted pulse waveforms can then be simulated efficiently. Examples of simulated sonar maps of two floor plans illustrate the performance of the model. Actual sonar maps are presented to verify the simulation results.

1 Introduction

Acoustic sensors provide an inexpensive means for determining the proximity of objects. Such sensors have shown particular use in implementing sonar systems for mobile robot navigation.[1,2] One commonly employed implementation is the *time-of-flight (TOF)* system, which has been efficiently packaged by the Polaroid Corporation.[3] However, the main problem with sonar ranging systems is that they produce complex signals that require some interpretation to be used successfully. Problems arise in the straight-forward, but naive, interpretation that if a TOF reading is produced, then an object must lie along the transducer line-of-sight at that range. Several researchers have attempted to take the TOF information available from a series of transducer orientations[2] and at different vantage points [1] to produce a sonar map. These *ad hoc* attempts produce maps that, outside of limited domains of robustness, can omit real obstacles and insert artifactual obstacles.

This paper presents a simulation model that clarifies the physical principles that act to generate the signals that eventually produce the TOF reading. The results of the simulation model should assist sonar system users to interpret the observed readings. These interpretations will then lead to better use of TOF readings for sonar map production. The simulation model will also allow researchers to understand the limitations of sonar systems. A physically-based model allows access to all the components which contribute to a TOF reading. This knowledge can lead to insights for achieving a more general solution to the inverse problem than that offered by the TOF implementation. Also, a good sensor simulation model may prove useful for developing navigation concepts without the need for much tedious experimentation with robot hardware.

To generate the simulation model, ideas from several diverse areas are incorporated, including linear system theory, acoustics and digital signal processing. From linear system theory[4] we take the concepts of impulse response and the superposition principle. From acoustics,[5] we use Huygen's Principle and the far-field approximation to determine the reflections from corners, edges and walls. Digital signal processing concepts[6] are employed to implement the simulation model in discrete-time on a digital computer.

To illustrate the salient effects of sonar ranging systems, we reduce the complexity of the environment to be explored by constructing a 2-D world model composed of only walls, corners (concave right angles between walls) and edges (convex right angles between walls). This model allows us to perform the simulation in an efficient manner, while producing results that are still insightful. Once defined, the floor plan can then be examined with different transducer types to test the effects of transducer dimensions and resonant frequency on the observed acoustic signals.

These signals can then be applied to a variety of object detection algorithms to generate a sonar map, although this paper is concerned primarily with the TOF algorithm.

In Section 2, we briefly describe the operation of a TOF ranging system. In Section 3, the impulse response approach employed for separating the effects of the transducer and the object are presented. Using these results, the impulse responses of walls, corners and edges are derived in Section 4. The procedure for generating a sonar map with the resulting corner, edge, wall and transducer (CEWT) model is explained in Section 5. Examples using two different floor plans are compared with actual sonar data to illustrate the performance of the CEWT model in Section 6. Several interesting features are examined as the threshold level and transducer frequency are varied. The paper concludes with several observations that are helpful in approaching the inverse problem.

2 Time-of-Flight Boundary Detection

The basic components that comprise a time-of-flight (TOF) ranging system are shown in Figure 1. An acoustic transducer which is a transmitter/receiver (T/R) transmits an acoustic signal into space. Upon encountering an object, a reflection, or *echo*, may be detected by the transducer acting as a receiver. An example of an echo from a single object is shown in Figure 1. A conventional TOF system produces a reading whenever the echo amplitude exceeds a preset threshold level, shown to occur at time t_o. A range measurement z_o is obtained from the round-trip time of flight:

$$z_o = ct_o / 2 \tag{1}$$

where c is the speed of sound in air (0.343 mm/μs at room temperature). To generate a sonar map, a TOF *dot* is placed at this range along the transducer line-of-sight, the transducer is then oriented at a new *azimuth* and the process is repeated by transmitting another pulse. When the transducer is rotated about a stationary point and TOF readings are acquired at constant increments in angle, the resulting map is called a *sector scan*. Rather than rotating the transducer, multiple fixed transducers can be mounted in a ring[1] and the system can be analyzed in exactly the same manner.

Several features should be noted about the above TOF system. If the detected signal does not exceed the threshold value, no TOF reading is registered. In this case, an arbitrary range value, such as zero or some large value, is produced. For systems in which the same physical transducer is used as both the transmitter and receiver, there is a small range interval during which the receiver is recuperating from the relatively large transmit signal transient and is not sensitive to the echos. Finally, the echo waveform shown in Figure 1 corresponds to a simple impulsive-voltage excitation of the transducer. Other, more complicated waveforms are sometimes employed to overcome specific

problems or to enhance the sensitivity to certain targets.[3] In this paper we consider only the simple pulse waveform.

By considering the TOF system several simplifications can be employed in the simulation. Since TOF systems operate on the first echo whose amplitude exceeds the threshold value, we can ignore multiple reflections from the same object, since these occur at later times than the first reflection. For a similar reason, signals that return to the receiver by bouncing off the floor and ceiling can be also ignored, allowing the use of a two-dimensional model. The case of muliple reflections that can occur when the beam is diverted by an oblique wall and then encounters reflecting objects is also a case that can produce a multiple reflection artifact,[7] but is beyond the scope of the model.

3 Impulse Response Approach

Using a linear system model, we can express the time waveform detected at the receiver output $r(t)$ as the convolution of two time functions:

$$r(t) = \int_{-\infty}^{\infty} p(\tau)h(t-\tau)\,d\tau \qquad (2)$$
$$= p(t) * h(t)$$

where $p(t)$ is the *pulse waveform* and $h(t)$ is the *impulse response*, which represents the contribution of the reflecting structures. The main advantage of this impulse response formulation is that it provides a partial separation between effects of transducer and reflector (Figure 2). This separation allows us to examine efficiently the same set of reflectors with transducers having different characteristics. Of theoretical interest, the impulse response of a reflecting object indicates the response that is obtained when the probing signal has an infinite bandwidth. Practical pulses represent the observation of the world through a limited bandwidth. In the next section we consider typical sonar pulse waveforms and then determine the impulse responses of walls, corners and edges.

3.1 Pulse Waveforms

The pulse waveforms we employ correspond to the echo from an ideal specular reflector, such as a normally-incident plane, located in the transducer *far-field*, or at range $z > a^2/\lambda$, where a is the transducer radius and λ is the wavelength of the radiation. A typical pulse waveform can be approximated by a sinusoid modulated by a Gaussian envelope:

$$p(t) = exp[-\frac{t^2}{2\sigma^2}]\, sin(2\pi f_R t),\ for\ -3\sigma \le t \le 3\sigma, \qquad (3)$$

where σ is a measure of the pulse duration and f_R is the *resonant frequency* of the transducer. Three waveforms that are produced by exciting transducers having different resonant frequencies are shown in Figure 3. Later, we illustrate how these pulse waveforms determine the beamwidth of the transducer.

3.2 Huygen's Principle

Huygen's principle[5] allows us to investigate the properties of receiving and transmitting apertures having arbitrary shapes by breaking each one up into elements that are small compared to the wavelength of the radiation. The principle is invoked to compute the impulse responses of the corner, edge and wall elements in the model.

In performing the analysis, it is intuitively helpful to view the transmitting/receiving aperture as separate transmitter and receiver apertures. Let us first consider the pair of elements from the transmitting and receiving apertures shown in Figure 4a. In the impulse response formulation, when the transmitting element is excited by an impulse, it emits an impulsive spherical wave that begins propagating outward. At time $t=2z/c$, the wavefront is detected by the receiving element, which responds by producing an impulsive output. If this configuration is modeled as a linear system, with the input being the signal applied to the transmitter and the output being the signal produced by the receiver, then the impulse response of the system is given by

$$h_0(t,z) = \frac{1}{2z}\delta(t-2z/c) \tag{4}$$

where the $1/2z$ factor describes the attenuation of the spherical wavefront amplitude in the far-field of the transducer[5] and $\delta(t)$ is the Dirac delta function.[4] Sonar system designers are aware of this attenuation and normally include an amplifier whose gain increases with time (range) in a linear fashion to compensate for this spreading loss. This amplifier then normalizes the impulse response to be

$$h_1(t,z) = \delta(t-2z/c). \tag{5}$$

To simplify the further analysis, we assume that such an amplifier is included within the receiving element. We also make the *far-field approximation*, which states that, by the time it reaches the receiving element, the spherical wavefront can be approximated by a planar wavefront. This means that the receiving element can be moved a small distance, equal to the aperture radius, in the transverse direction without changing the arrival time of the impulse. This far-field approximation simplifies the computation significantly and still produces reasonable results.

3.3 Impulse Response of Receiver Transducer

We can now apply the results of the previous section by constructing the receiving aperture by summing the outputs of N small receiving elements. Let us begin by considering two receiving elements located on a line that is inclined by angle α with respect to the wavefront propagation direction (Figure 4b). Since acoustic transducers constructed with a flexible membrane, typical of the Polaroid type,[3] are sensitive to normally-incident pressures, the output of each element must be scaled by an *obliquity factor*, equal to $\cos\alpha$. If the output of this system is taken as the sum of the signals produced by the receivers, then the system impulse response is given by

$$h_2(t,z,a,\alpha) = \{\delta(t-\frac{2z - a\sin\alpha}{c}) + \delta(t-\frac{2z + a\sin\alpha}{c})\}\cos\alpha \tag{6}$$

where 2a is the separation between the receiving elements.

A circular receiving aperture can be approximated by arranging N elements in a rectangular grid with horizontal rows and vertical columns (Figure 5). When the transmitting element transmits an impulse, after the travel time $t=2z/c$, the receiver detects the signal with all N elements. With the far-field approximation, all the elements detect the signal simultaneously when the aperture is normally incident to the propagation of the signal, thus producing an impulse of weight N. When the receiver aperture is inclined by angle α, some of the rows of receiving elements are closer to the transmitter than others. Hence, the wavefront propagates across the receiver aperture in a finite time, causing the impulse response to be spread out in time. To obtain a continuous-time function for the impulse response, we make a limiting argument in which the size of the elements decreases while their number increases to maintain a constant output. For a circular aperture, the receiving aperture impulse response, denoted by $h_R(t,z,a,\alpha)$ has the form of the positive half of an ellipse:

$$h_R(t,z,a,\alpha) = \frac{\cos\alpha}{v}[1 - w^2(t - 2z/c)^2]^{1/2} \tag{7}$$
$$for\ \frac{2z-a\sin\alpha}{c} \le t \le \frac{2z+a\sin\alpha}{c}\ and\ 0<|\alpha|\le\pi/2,$$

where v and w are constants to be determined by employing the following two constraints. If the obliquity factor is ignored, the area under the impulse response curve is equal for all values of α, since all the elements detect the impulse. This area has been normalized to unity in the model. The second constraint is that $h_R(\frac{2z\pm a\sin\alpha}{c},z,a,\alpha) = 0$. Applying these constraints, we get

$$h_R(t,z,,a,\alpha) = \frac{2c\cos\alpha}{\pi a\sin\alpha}\left(1 - \frac{c^2(t-2z/c)^2}{a^2\sin^2\alpha}\right)^{1/2}, \tag{8}$$

$$\text{for } \frac{2z-a\sin\alpha}{c} \le t \le \frac{2z+a\sin\alpha}{c} \text{ and } 0 < |\alpha| \le \pi/2,$$

$$h_R(t,z,a,0) = \delta(t-2z/c), \quad \text{for } \alpha = 0,$$

and

$$h_R(t,z,a,\alpha) = 0, \quad \text{otherwise.}$$

In the next section, we apply a similar procedure to the transmitting aperture to determine the impulse response of the T/R in terms of Eq. (8).

3.4 Impulse Response of T/R Pair

As in the previous section, we construct a circular transmitting aperture by connecting N small elements (Figure 6). Since we are ultimately concerned with pulse/echo sonar systems, the transmitting aperture has the same shape as the receiver. When both apertures are normal to the propagation direction ($\alpha = 0$), the impulse response of the T/R pair, denoted by $h_{T/R}(t,z,a,\alpha)$, is concentrated at t = 2z/c:

$$h_{T/R}(t,z,a,0) = N^2\,\delta(t-2z/c). \tag{9}$$

As above, we normalize the area under the impulse response to unity. When the apertures are oblique, it is convenient to have the transmitter and the receiver inclined by the same angle. We note that the elements in a particular row in the transmitter contribute to the same impulse, whose weight depends on the number of elements in the row, and whose relative time position depends on the location of the row. Because of the similarity in the shapes of the two apertures, the effect of these weighted and delayed transmitted impulses on the output signal can be described by the self-convolution of the receiver impulse response $h_R(t,z,a,\alpha)$, to yield

$$h_{T/R}(t,z,a,\alpha) = \int_{\frac{2z-a\sin\alpha}{c}}^{\frac{2z+a\sin\alpha}{c}} h_R(\tau,z,a,\alpha)\,h_R(t-\tau,z,a,\alpha)\,d\tau \tag{10}$$

Although the integral solution can be found with the help of tables,[8] it is very complicated and provides little insight. The numerical evaluation of (10) is straight-forward once $h_R(t,z,a,\alpha)$ is evaluated

in suitably small discrete-time increments, e.g., 1 μs. Figure 7 shows the results as the inclination angle α is varied. Note that the impulse response amplitude decreases and its duration increases with α. Also note that because both apertures are limited in extent, $h_{T/R}(t,z,a,\alpha)$ is zero outside the range $\frac{2z-2a\sin\alpha}{c} \le t \le \frac{2z+2a\sin\alpha}{c}$.

The importance of (10) is that it gives the impulse response of the T/R pair in closed analytic form in terms of the transducer radius a and inclination angle α. This obviates the need to perform the otherwise time-consuming operation of calculating the impulse response by the standard Huygen's approach, which requires a summation of the time delayed responses in an element-by-element fashion. In the next section we show that (10) is exactly the result that is required to determine the impulse responses for walls, corners and edges.

4 Reflections from Walls, Corners and Edges

The results derived above are now applied directly to the situation encountered in the sonar ranging problem to determine the impulse responses produced by walls, corners and edges.

4.1 Reflection from a Wall

We assume that the acoustic reflection from a wall is lossless, so that it appears like a perfect mirror to the acoustic waves. For this case, the single T/R transducer can be modeled by separate transmitting and receiving apertures (Figure 8). Note that this configuration is exactly the one considered above. Hence, the impulse response of a wall inclined by angle α with respect to the transducer orientation, denoted by $h_W(t,z,a,\alpha)$, is given by

$$h_W(t,z,a,\alpha) = h_{T/R}(t,z,a,\alpha). \tag{11}$$

Note that by separating the two apertures it becomes apparent that only the reflections from the normally incident parts of a wall are detected. Further, by drawing lines connecting the extremes of the two apertures, it is apparent which parts of the wall contribute to the reflected signal. This procedure can be used to determine the minimum size of the wall in our model.

Modeling the plane as a mirror allows us to find a set of unique signal paths from the transmitter to the receiver. Such unique paths do not exist for reflectors having rough surfaces, since there may be many paths that lead from the transmitter to the receiver. Since such rough surfaced reflectors would greatly complicate the model, they are excluded. This exclusion, however, does not severely limit the insights provided by the model: laboratory simulated environments (see Figure 14) and simple real world environments[9] have proven to be more acoustically specular than might be guessed *a priori*.

4.2 Reflection from a Corner

In our model, a corner is defined by the line between two perpendicular walls that form a concave dihedral (Figure 9). The location and orientation of the transducer with respect to the corner is determined by the line drawn from the center of the aperture to the location of the edge. Since the reflection from the walls is lossless, the corner acts like a two-dimensional corner-cube reflector. Modeling the T/R transducer as a separate transmitter and receiver produces the configuration shown in Figure 9. By tracing the ray lengths we find that the angle of inclination of the equivalent receiver aperture is the negative of that for the wall (Figure 8).

By our far-field approximation, the transmitted impulses are a series of weighted plane waves that propagate across the receiver aperture. Because of the symmetry of the circular shape, the form of the detected signal is the same as that in the case of the wall, making the sign of the inclination angle irrelevant. Hence, the impulse response of a corner, $h_C(t,z,a,\alpha)$, is identical to that of a wall:

$$h_C(t,z,a,\alpha) = h_{T/R}(t,z,a,\alpha). \tag{12}$$

A slight simplification has been made in arriving at (12): In addition to the *reflected* signal, there is a second component to the signal scattered from the corner, the *diffracted* signal, which originates from the line of intersection between the two walls defining the corner. In the case of the corner, this diffracted signal is much smaller than the reflection, and is hence ignored. However, in the case of the edge, considered next, it is *only* this diffracted wave that is detected at the receiver.

4.3 Reflection from an Edge

Whereas the plane and corner can be sensed by reflected signals, the edge produces a diffracted signal, which is a cylindrical wave that seems to be emanating from the edge location (Figure 10). To approximate the magnitude of the diffracted cylindrical wave, we model the edge as a rigid knife-edge and employ the result known from acoustics:[5]

$$h_E(t,z,a,\alpha,\lambda) = \frac{2h_{T/R}(t,z,a,\alpha)}{4\pi\sqrt{z/\lambda}}. \tag{13}$$

To obtain this approximation, we make a *narrow-band* assumption that the gain is constant over the bandwidth of the transducer. This allows us to use the impulse response approach by assigning a gain factor proportional to $\sqrt{\lambda}$ to each transducer. The above form also contains the cylindrical wave amplitude attenuation factor $\sqrt{1/z}$. The explicit factor 2 in the numerator is from the range compensation gain amplifier in the receiver.

Aside from the magnitude factor, the form of $h_{\ell}(t,z,a,\alpha)$ is identical to those from the corner and edge, since an identical set of a delayed and scaled plane waves passes over the receiver aperture in this case as well. However, while walls and corners are equally visible independent of distance, edges become invisible as $\sqrt{1/z}$.

4.4 Beam Pattern

We use the impulse response results to determine the beam pattern of a transducer. The standard *beam pattern* of a transducer is obtained by monitoring the magnitude of the signal reflected from a point target, which reflects isotropically in all directions, as the transducer is rotated through a set of inclination angles. This concept of beamwidth cannot be directly related to walls, corners and edges, which have a directionality to their reflections, although it would be useful to determine the range of inclination angles for which an element is still detectable. This type of beam pattern can be determined from the waveforms obtained by convolving the pulses shown in Figure 3, with the impulse responses shown in Figure 7. The set of such curves is shown in Figure 11. Note that the maximum amplitude of the detected reflection decreases both with the inclination angle α and with the transducer resonant frequency. Since an element is detected when the reflected signal exceeds the threshold level, we see that the beam width decreases for the higher frequency transducers. This effect is illustrated in the examples below.

5 Corner-Edge-Wall-Transducer [CEWT] Model

Having determined the acoustic signals that are reflected from the corner, edge and wall, we have all the components necessary for our CEWT simulation model. In this section, we describe the steps for laying out a floor plan and running the simulation. The simulation procedure occurs in several discrete steps to allow for an efficiency of computation when investigating the results of varying a particular parameter. Examples below show the effect of changing the threshold value and transducer resonant frequency.

5.1 Floor Plan Code

The first step in the simulation is to specify the floor plan of the space in which our sonar system operates. For the elements in our two-dimensional floor plan, we allow only walls that are parallel to the x- and y-axes, and the edges and corners that can be formed with these walls. The floor plan is designed by specifying mutually consistent locations of corners, edges and walls.

In describing the floor plan we are interested in representing the information in a manner that allows us to determine the reflected signals in an efficient manner. The floor plan is represented in terms of

the *elements* (walls, corners, edges) that contribute to the impulse response of the T/R at every interior location. In our model, each pixel in the interior space is represented by a 31-bit (positive integer) word coded with element *visibility*: If the n^{th} element is visible from a particular pixel position, then the n^{th} bit in the corresponding word is set to one. For a wall to be visible, the T/R location within the space must have an unobstructed perpendicular projection to that wall. For corners and edges to be visible, the T/R must have a unobstructed line-of-sight to their location. The pixel values of the walls are set to a negative value (-1) to delimit the space.

Shadows are regions in the floor plan from which not all elements are visible. The edges determine the shadow regions by blocking the line-of-sight of the T/R to a particular element. These shadow regions are found by exhaustive search after the floor plan is specified. Examples of shadow regions are shown in Figure 12. Shadow boundaries for walls are produced by edges that block the perpendicular projection of the T/R. The visible region for a given wall is found by projecting the wall into the interior space and reducing the projection width monotonically as an edge is encountered. The shadow boundaries for corners and edges are produced by edges that block their direct line-of-sight by the T/R. The shadow region for a corner is generated by computing the slope of the line connecting the corner to the blocking edge, and setting the corner bit to zero in the floor plan pixels lying on the appropriate side of the line and past the blocking edge. Note that, unlike a corner, which can be viewed from only one quadrant, an edge can be viewed from three quadrants. The edge shadow region is most easily generated by employing the corner algorithm above to the three quadrants of view.

The shadow regions in Figure 12 were found by assuming the T/R radius to be zero. To include the effects of the transducer radius, the wall shadows should be decreased by the radius. This effect is negligibly small if the room is large compared to the transducer dimensions, which is almost always the case in practice.

5.2 Detected time waveform

Having determined the floor plan and shadow regions, the T/R location, radius and orientation is specified to determine the impulse response from the visible elements by using Eqs. (11), (12) or (13). Being restricted by the obliquity factor in Eq. (8), only the visible elements within $\pm 90^{o}$ of the T/R orientation contribute to the *total impulse response*, which is obtained by summing the individual element responses. The *detected signal waveform* is obtained by convolving this total impulse response with the pulse waveform, as shown below. A range reading is calculated from the time at which this detected signal first exceeds the specified threshold level. If the threshold is never

exceeded a zero valued range is returned. The location of the TOF dot is placed at the calculated range, at the azimuth corresponding to the transducer orientation. A *sector sonar map* is generated by rotating the transducer in a complete rotation in small angular increments (2^o).

5.3 CEWT Model Parameters

To simulate a sonar ranging system, the following values were employed in our CEWT model for the various physical parameters.

The maximum area of the floor plan was a square space defined by 128 x 128 element grid, corresponding to 1.28 m by 1.28 m. This imposes a 1 cm resolution for the element and T/R locations. The T/R ranging resolution was determined by the sampling rate of the analog signals, which was chosen to be $f_s = 1$ MHz. This high rate was necessary to retain the shape of the impulse responses of the three types of elements. If the sampling period is given by T_s ($= 1/f_s$), the spacial resolution represented by this sampling rate is equal to $cT_s/2 = 0.17$ mm. The size to be allowed for the impulse response array is determined by the maximum possible round-trip travel time of any reflection, which occurs along the diagonal, requiring 10,565 elements at the 1 MHz sampling rate. The T/R radius was chosen to be 20 mm, identical to the Polaroid transducer. In addition to the 60 KHz resonant frequency, typical for the Polaroid, two additional frequencies were considered (30 and 120 KHz) to investigate the effects of changing frequencies.

The threshold level was specified relative to the amplitude of the echo from a normally-incident wall. Because of the range compensated amplifier gain, this signal level is constant with range. Threshold levels of -20 dB (1/10 the amplitude), -40 dB (1/100) and -60 dB (1/1000) are specified and the difference in the sonar maps observed. Although current practical sonar systems operate between -20 and -40 dB, the -60 dB level is interesting because it illustrates the pitfalls encountered in designing such a sensitive system.

The simulation was implemented on a VAX-750 programmed in the C-language. To determine the shadow regions in the floor plan required a maximum of ten minutes of CPU time. To generate the complete sonar sector maps shown below required between 10 and 40 minutes, spent mostly on the convolution of the impulse response with the pulse waveform. Hence, this time was strongly dependent on the range difference between the nearest and farthest elements from the T/R.

6 Simulation Model Results

We now show the results obtained by scanning two floor plans CEW0 and CEW1. CEW0 is the simplest possible which contains all three element types. Its purpose is to illustrate some of the basic features of the model and to be compared with actual sonar maps. The more interesting CEW1 is a more complicated floor plan to illustrate the subtle effects that can occur with sonar ranging systems.

6.1 Discussion of CEW0 Results

The results of scanning CEW0 with the three different threshold settings are shown in Figure 13. To verify the validity of the simulation model, actual results produced with the Polaroid sensor are shown in Figure 14. The actual scans are shown for threshold values of -20 and -36 dB, the latter being the capability of the experimental equipment. Note that, for both real and simulated sonar maps, the corners indeed generate patterns that are identical to walls, and that the edge is detected at the two more sensitive threshold settings, but is invisible at the lowest sensitivity.

6.1.1 Beam Patterns

By locating the T/R in the lower left of the space, we are able to observe the effects of range on the sonar map. Recall that the TOF range dots appear along the transducer line-of-sight at the location corresponding to where the threshold was exceeded, and that the reflected signal magnitude decreases with the magnitude of the inclination angle α. If no dot appears, the detected signal did not exceed the threshold level. At the least sensitive threshold setting (-20 dB), the threshold is exceeded when $|\alpha|<6^o$, producing the narrowest beam width. At the -40 dB threshold level, the threshold is exceeded for $|\alpha|<15^o$, and the signal from the edge is detected. At the most sensitive threshold setting (-60 dB), a signal is detected at almost every T/R orientation. Since the TOF dot is placed along the T/R line-of-sight, but the normal distance between the T/R and the reflecting element is constant with respect to the inclination angle, the sonar map consists of arcs. The observation that the arcs are not of strictly constant radius is an artifact of the pulse waveform and thresholding process. The larger jumps between arcs are described in the next section.

6.1.2 Range Jumps

The -60 dB level is so sensitive that TOF dot appears at almost every T/R orientation. It is interesting to investigate the cause of the large jumps in the TOF range reading that occur for small changes in T/R orientation. Such a jump occurs when the transducer orientation changes from 26^o to 30^o (Figure 13). The impulse response and detected signal waveforms are shown in Figure 15. Note that small changes in the transducer orientation shift the amplitudes of the impulse response components from the visible elements. The sensitivity of the nonlinear TOF processing is evident for signals that have amplitudes that are close to the threshold level.

6.1.3 Different Frequency Transducers

The results of scanning CEW0 with three different resonant frequencies and the same threshold level (-40 dB) are shown in Figure 16. As was illustrated in Figure 11, for a given threshold setting, the maximum angle of inclination for which the reflected signal amplitude exceeds the threshold is inversely related to the resonant frequency. This results in a beamwidth that is inversely related to resonant frequency. We note that to a first-order approximation, reducing the transducer frequency produces results that are similar to lowering the threshold level.

6.2 Discussion of CEW1 Results

The results of scanning CEW1 with the different threshold settings are shown in Figure 17. The same observations made above are also true here. An additional effect is evident from this more complicated floor plan. Because the TOF processing returns the range of the first detected signal that exceeds the threshold level, it is possible that much larger signals occurring at later times are not detected. This results in a *shielding* of some of the more remote elements by those more proximal, as illustrated in the lower left corner of CEW1 and the edge between it and the T/R. This effect adds to the difficulty of interpreting sonar maps obtained with this commonly used TOF scheme.

7 Conclusions

This paper has described a physically-based simulation model for assisting in the interpretation of sonar ranging systems. An insight important for visualizing the behavior of acoustic transducers is that the T/R transducer can be separated for analytical purposes into separate transmitter and receiver apertures. The computational efficiency of the model is due in large part to the assumption of mirror-like reflectors, for which we have analytic closed-form solutions for the impulse responses for the wall, corner and edge.

The results of the CEWT (corner-edge-wall-transducer) model demonstrate the following:

- An isolated *element* (wall, corner or edge) generates an arc whose angular extent is determined by the threshold setting and resonant frequency of the transducer. The true location of the reflecting portion of an isolated element is at the angular center of the arc. For an edge, the arc length is also a function of the ratio of its distance from the T/R to the acoustic wavelength of the probing pulse.

- From a *single* reflected signal, it is impossible to differentiate corners, edges and walls, since the forms of their impulse responses are identical.

- From the set of signals from a *single* sector scan:

    - at minimal threshold sensitivity (-20 dB),

- beamwidth is the narrowest,
- corners and edges are detected at approximately normal incidence ($|\alpha|<6^o$), but cannot be differentiated,
- edges are detectable only at close range, because of the $\sqrt{1/z}$ amplitude loss.

o at maximal threshold sensitivity (-60 dB),

- beamwidth is the widest,
- edges are observed,
- there is almost always a TOF reading, usually from the closest element,
- shielding of farther elements by more proximal elements often occurs.

- From the set of signals using *multiple* sector scans, each from a different vantage point (*compound scan*):

o in CEW world, corners are determined by extending walls and applying consistency rules, and edges are detected by their $\sqrt{1/z}$ amplitude characteristic,

o in the general situation, the problem is still wide open, with the solution dependent on the cleverness and insights of the designer.

The organization of the model allows an efficiency of computation for investigating different aspects of the problem. The shadow regions of the floor plan are determined first and are applicable for a wide range of T/R types. To determine the impulse response of the floor plan elements for a particular T/R location, only the transducer radius need be specified. Different transducer resonant frequencies and transmitted waveforms can be tested by convolving the set of impulse response sequences for the various T/R orientations with the appropriate pulse waveform to generate the detected time waveforms. Posing the solution in the intermediate form of the total impulse response allows the investigation of the ideal case of infinite bandwidth pulse waveforms. All other practical waveforms can be viewed as observing this impulse response through a limited bandwidth. Finally, the effects of varying the threshold can be observed by processing these detected signals.

8 Acknowledgments

The actual sonar maps were produced by Du-Juan Di, currently at the Digital Signal Processing Laboratory in the Department of Electrical Engineering at Yale University. The assistance in the CMU Robotics Intelligent Sensors Laboratory of Mark Hahn in programming the simulation model and Alan Guisewite in solving the practical problems are gratefully acknowledged. This work was performed during the first author's sabbatical leave at The Robotics Institute at Carnegie-Mellon University.

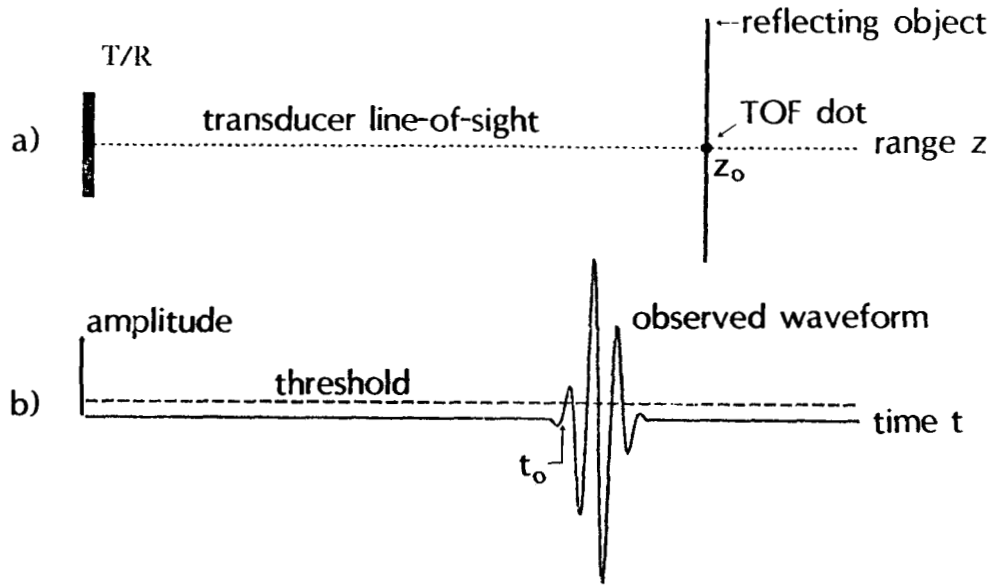

Figure 1: Components of a time-of-flight (TOF) ranging system. *a*) Physical configuration. *b*) Time waveforms.

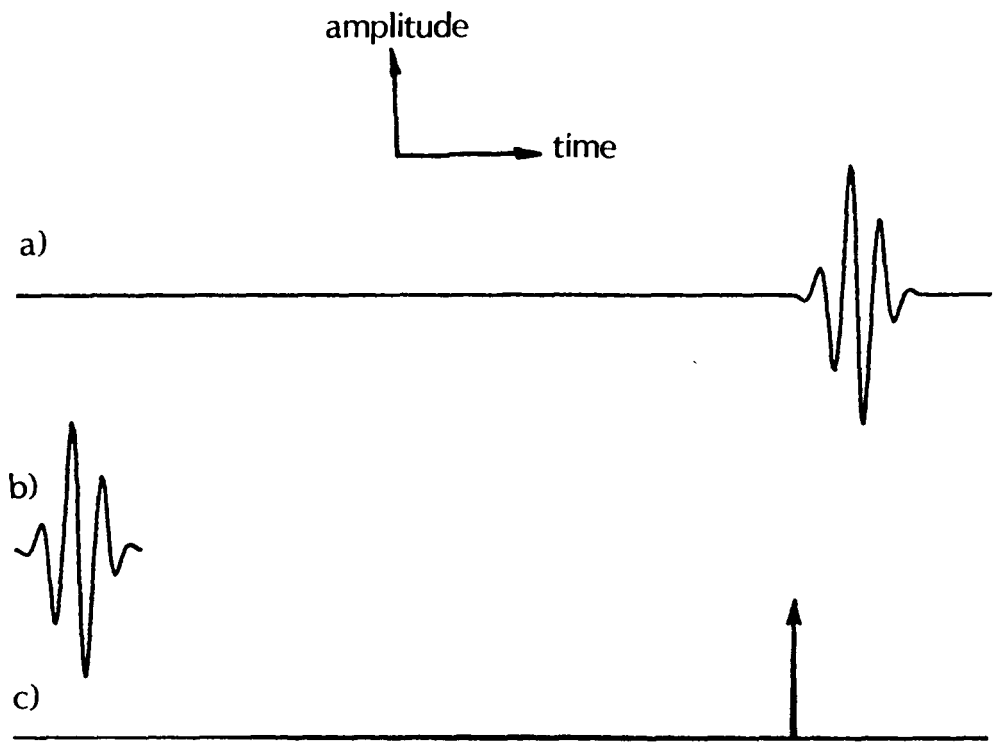

Figure 2: Impulse response approach. *a*) Observed time waveform r(t), *b*) Pulse time waveform p(t), *c*) Impulse response time waveform h(t).

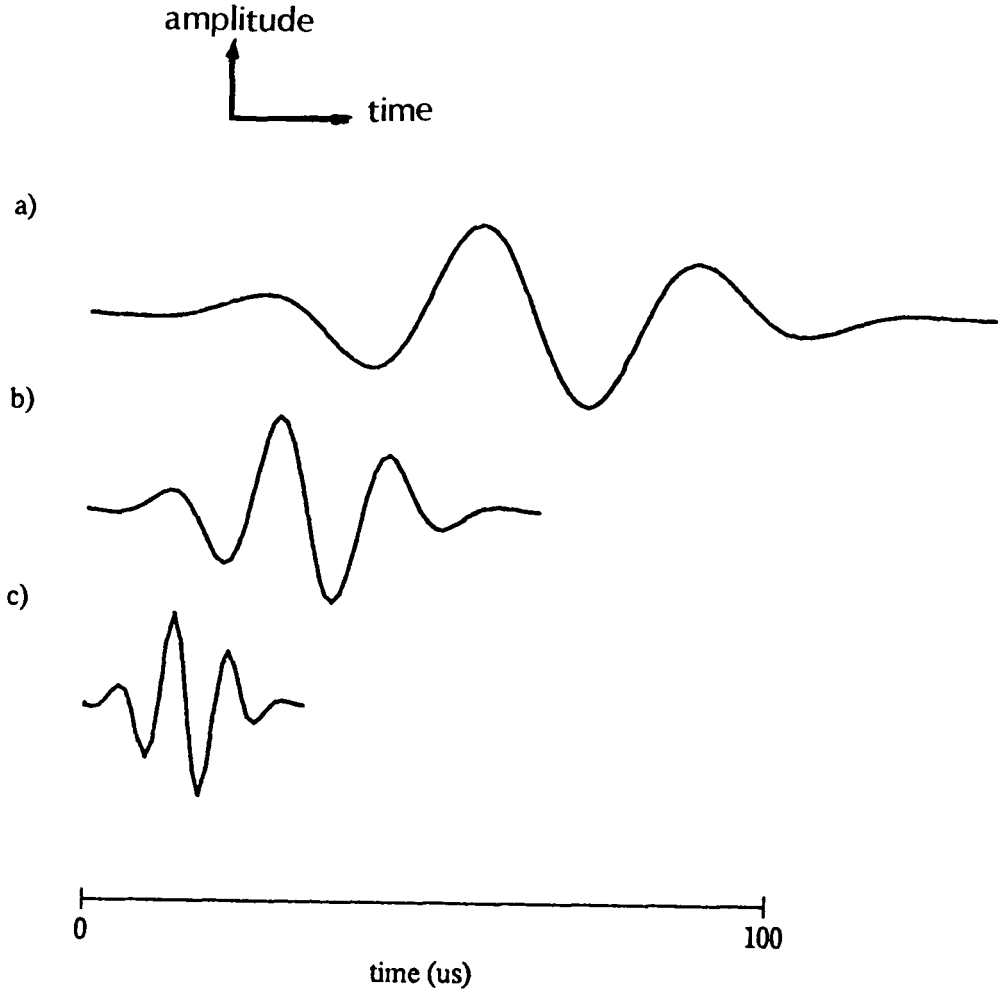

Figure 3: Typical pulse waveforms for three transducers of different resonant frequencies: *a*) $f_R = 30$ KHz, *b*) $f_R = 60$ KHz, *c*) $f_R = 120$ KHz.

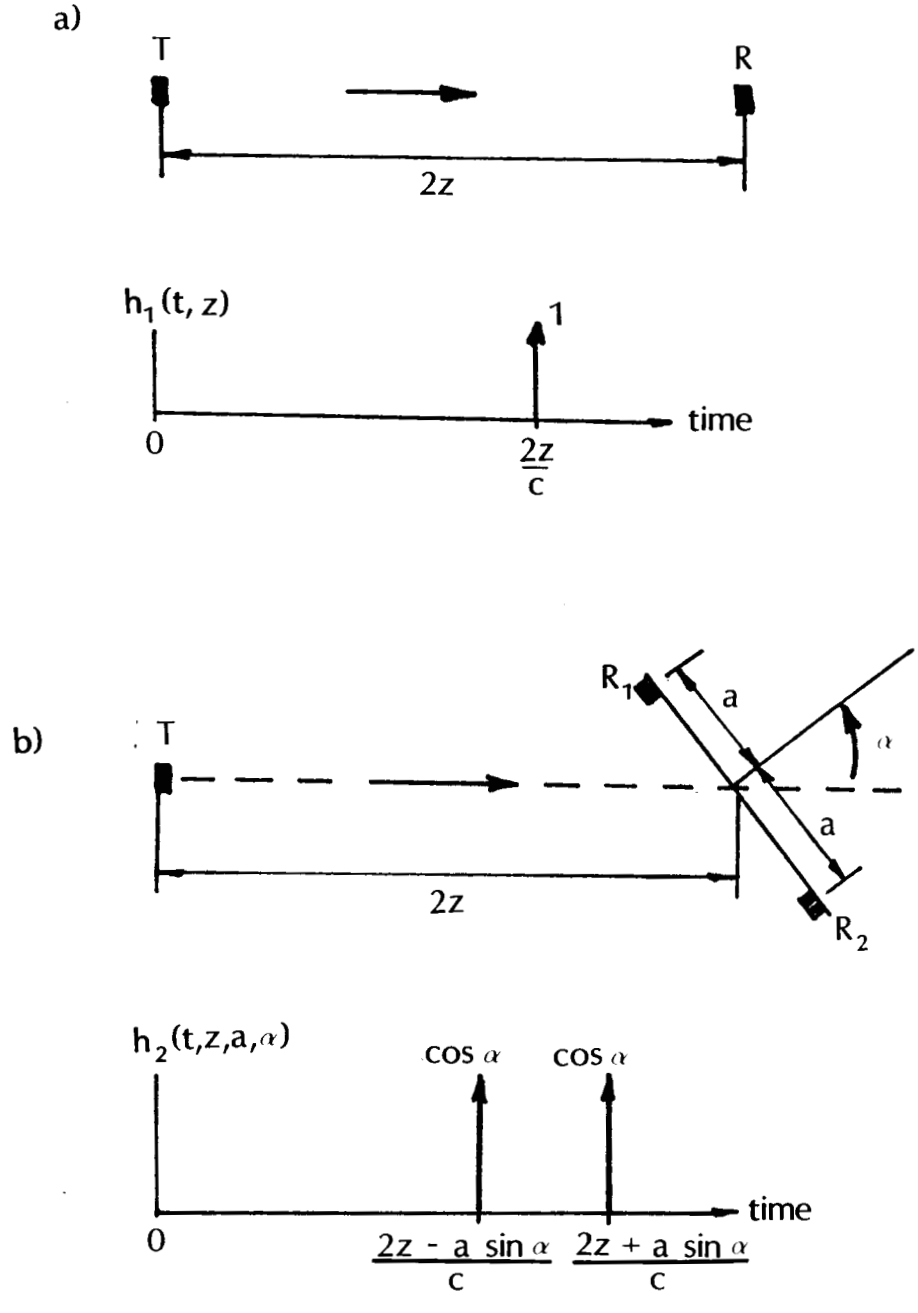

Figure 4: Huygen's elements and corresponding impulse response waveforms:
a) Single transmitting (T) and receiving (R) elements,
b) Two receiving elements
separated by distance 2a and inclined by angle α with respect
to direction of propagation.

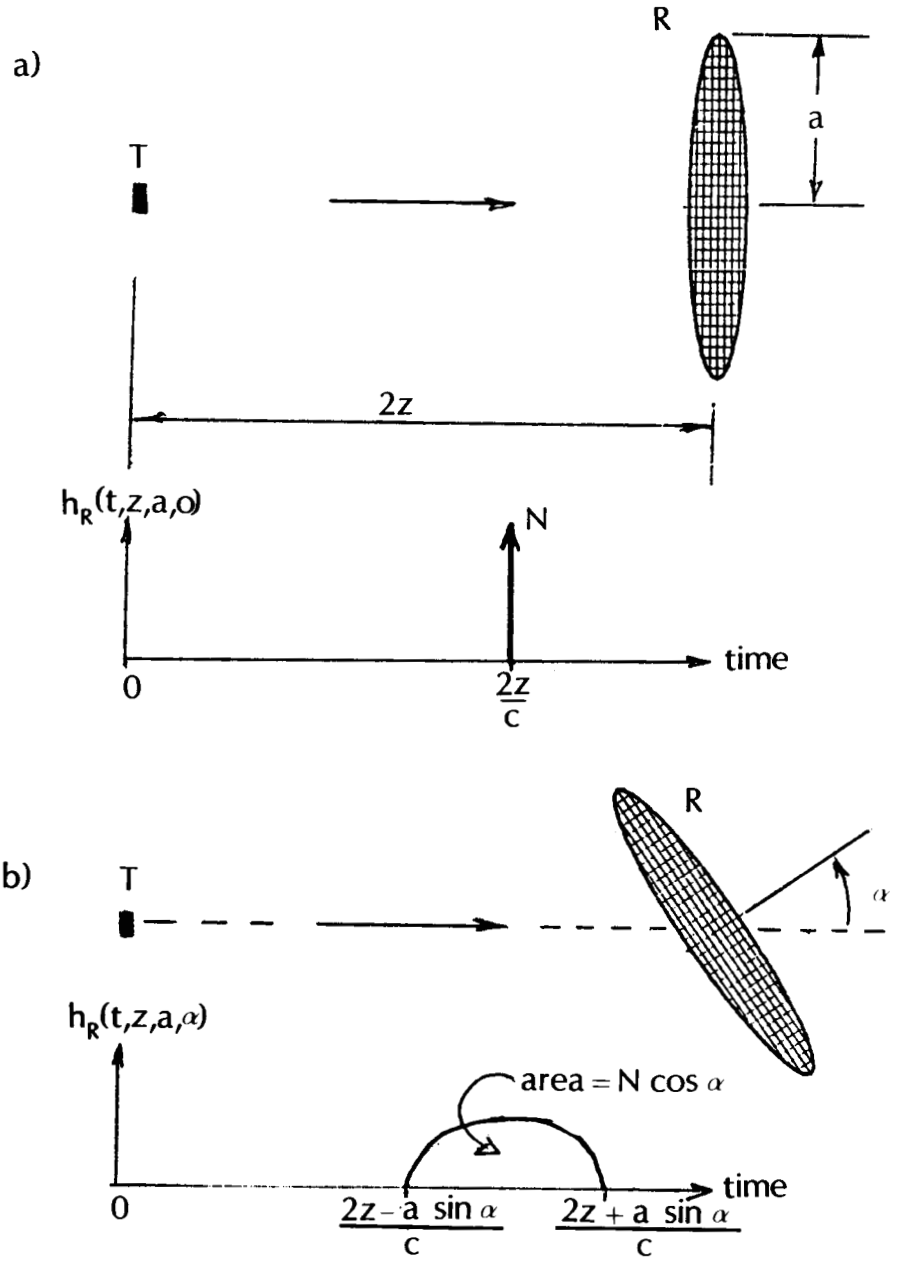

Figure 5: Impulse response for receiver aperture: *a*) Normal incidence, *b*) Oblique incidence.

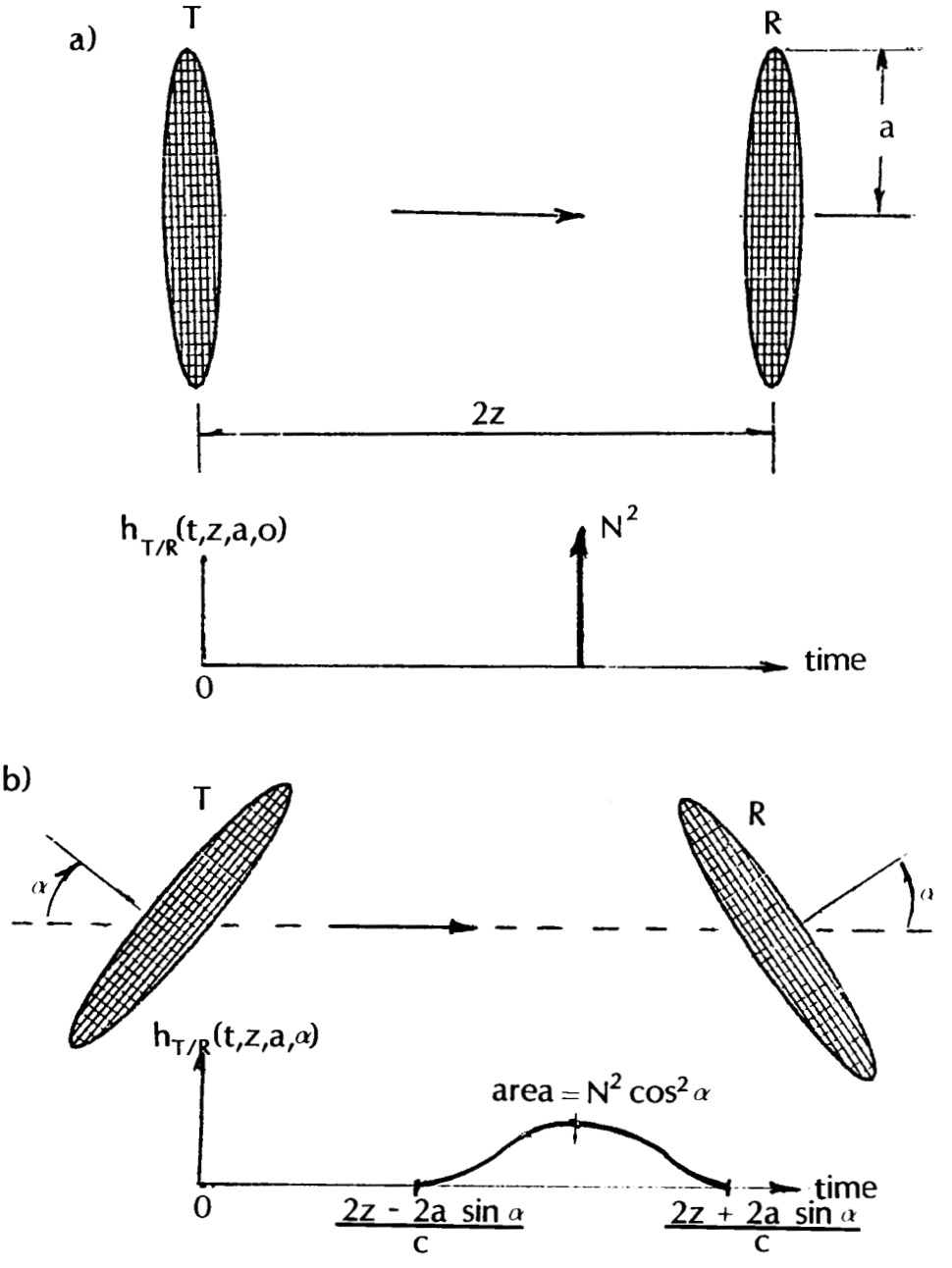

Figure 6: Impulse response of T/R pair: *a*) Normal incidence, *b*) Oblique incidence.

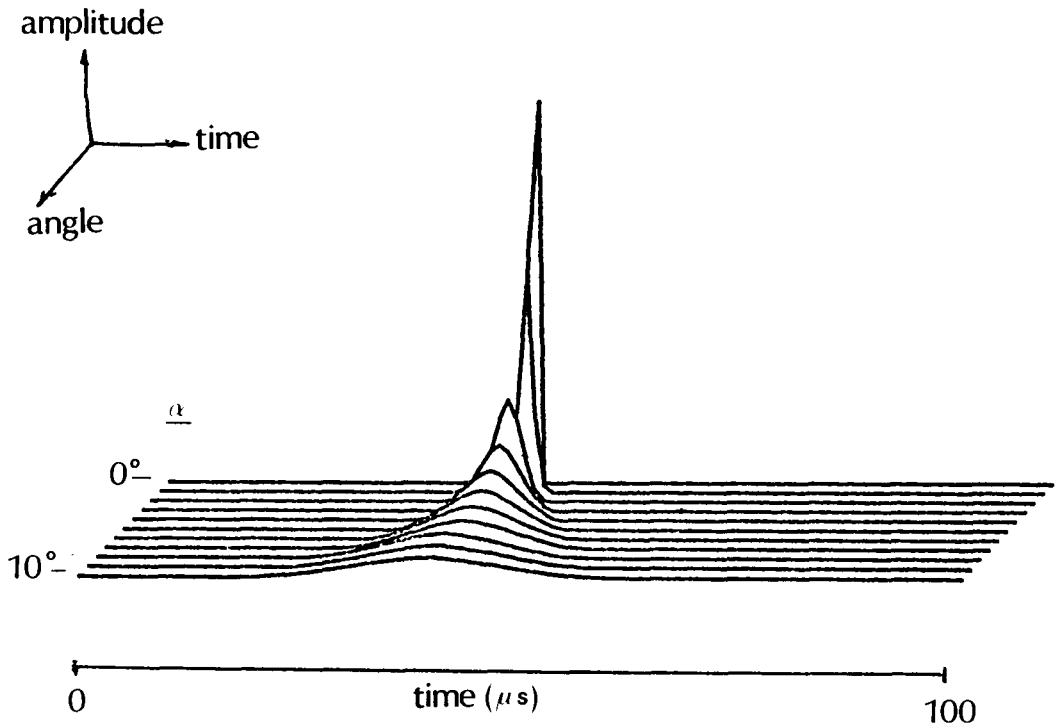

Figure 7: T/R impulse response waveforms plotted with inclination angle α as parameter. (transducer radius = 20 mm).

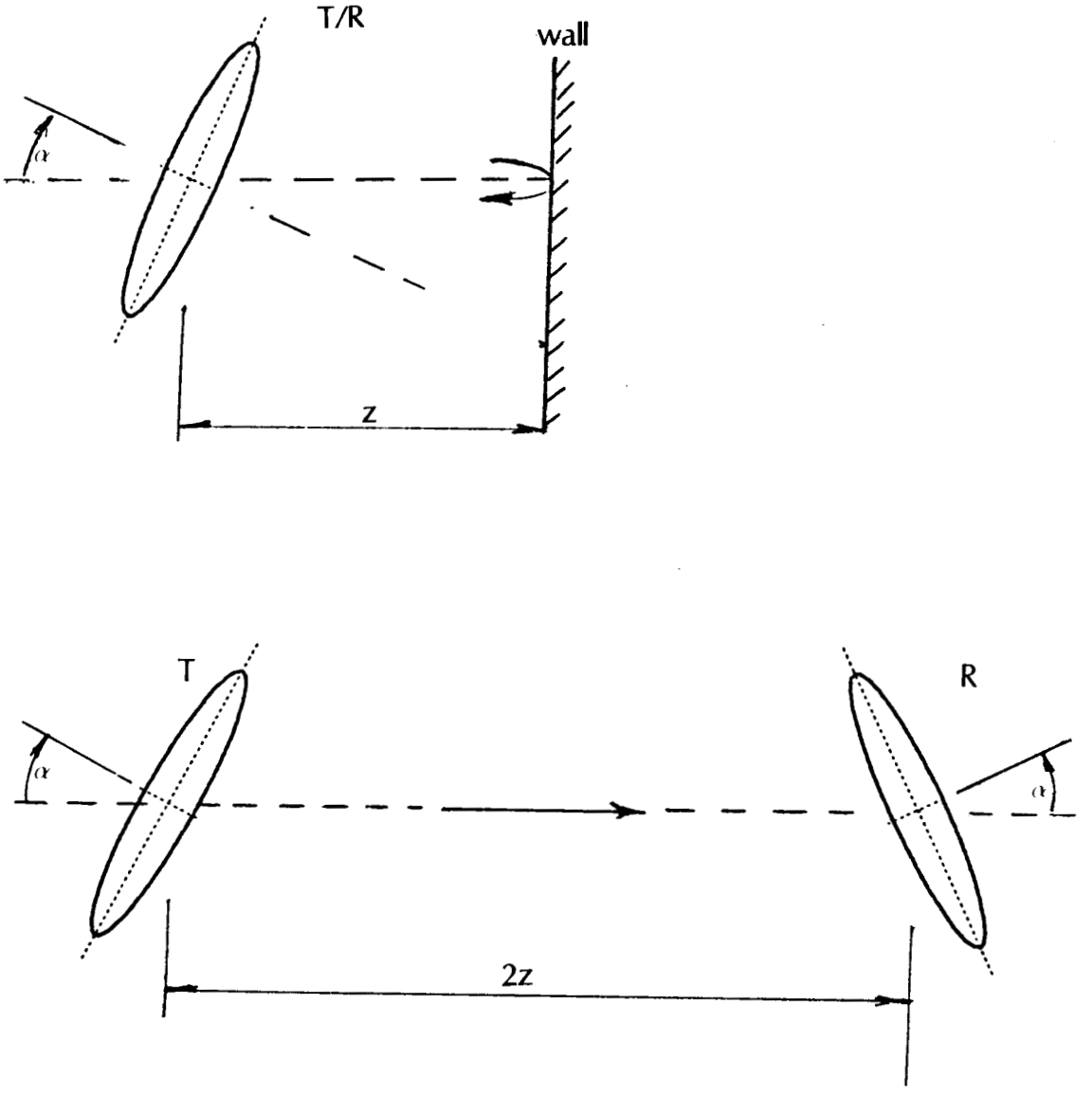

Figure 8: Separation of T/R into transmitter and receiver for wall reflections.

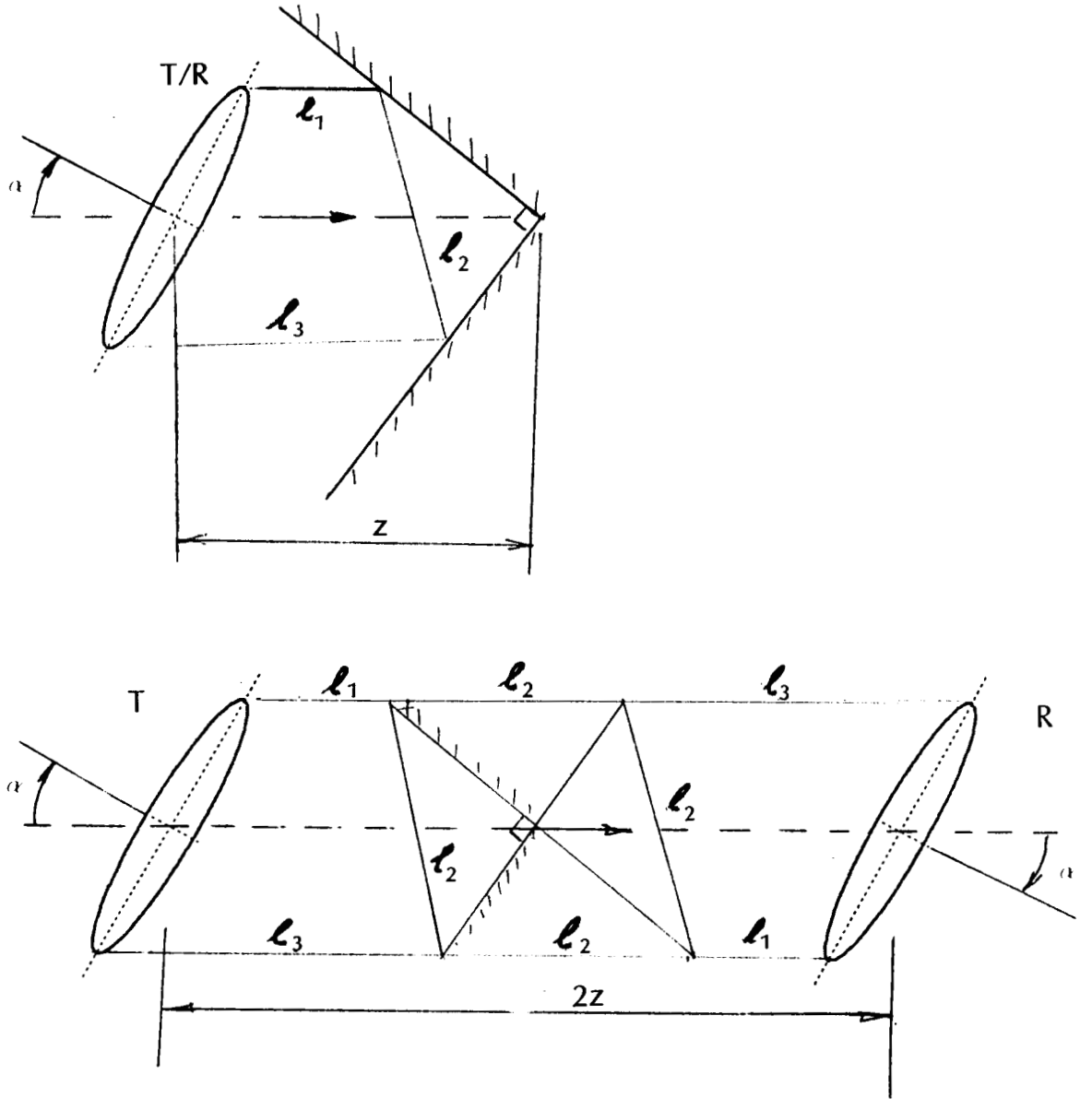

Figure 9: Separation of T/R into transmitter and receiver for corner reflections.

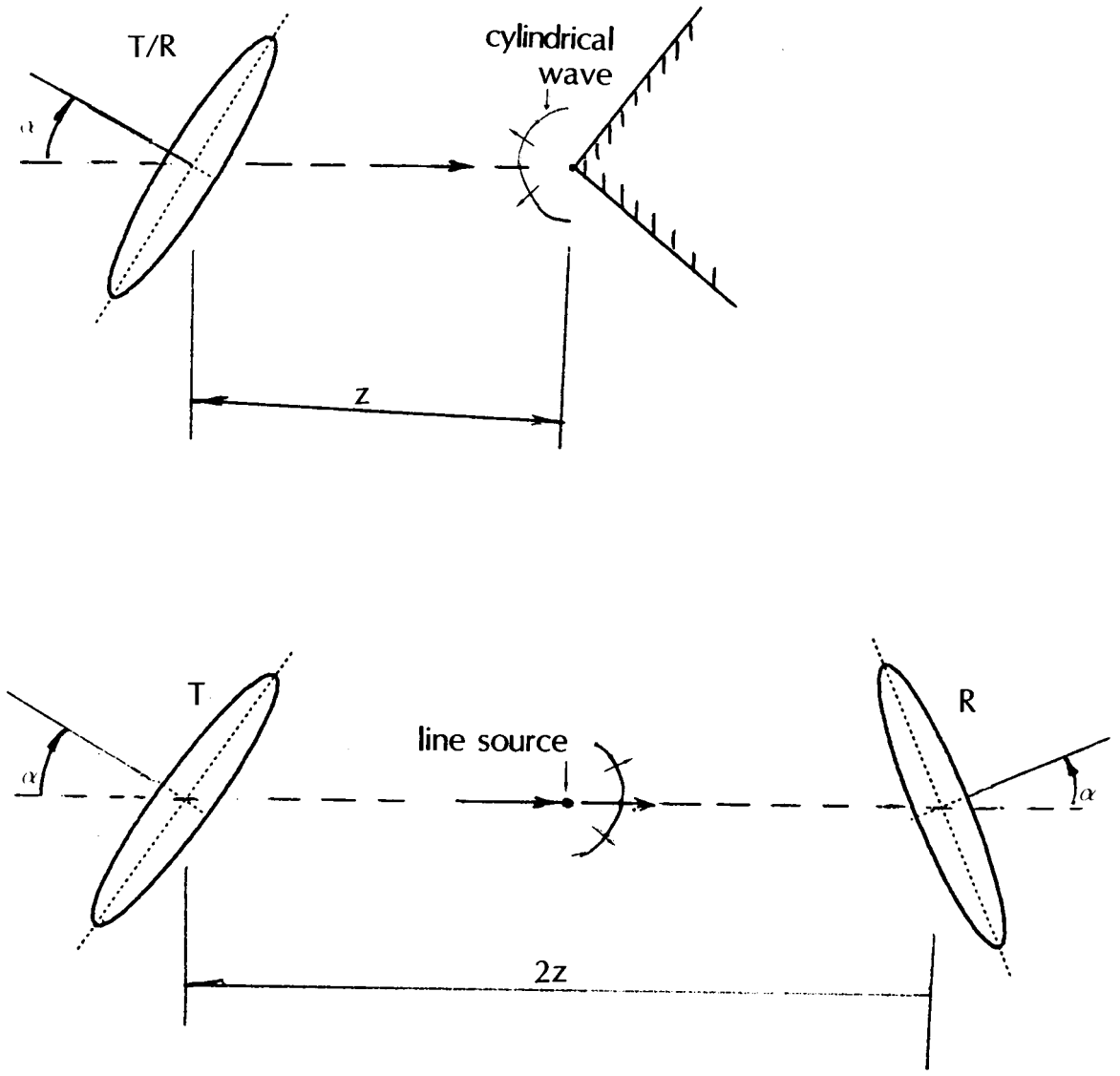

Figure 10: Separation of T/R into transmitter and receiver for edge reflections.

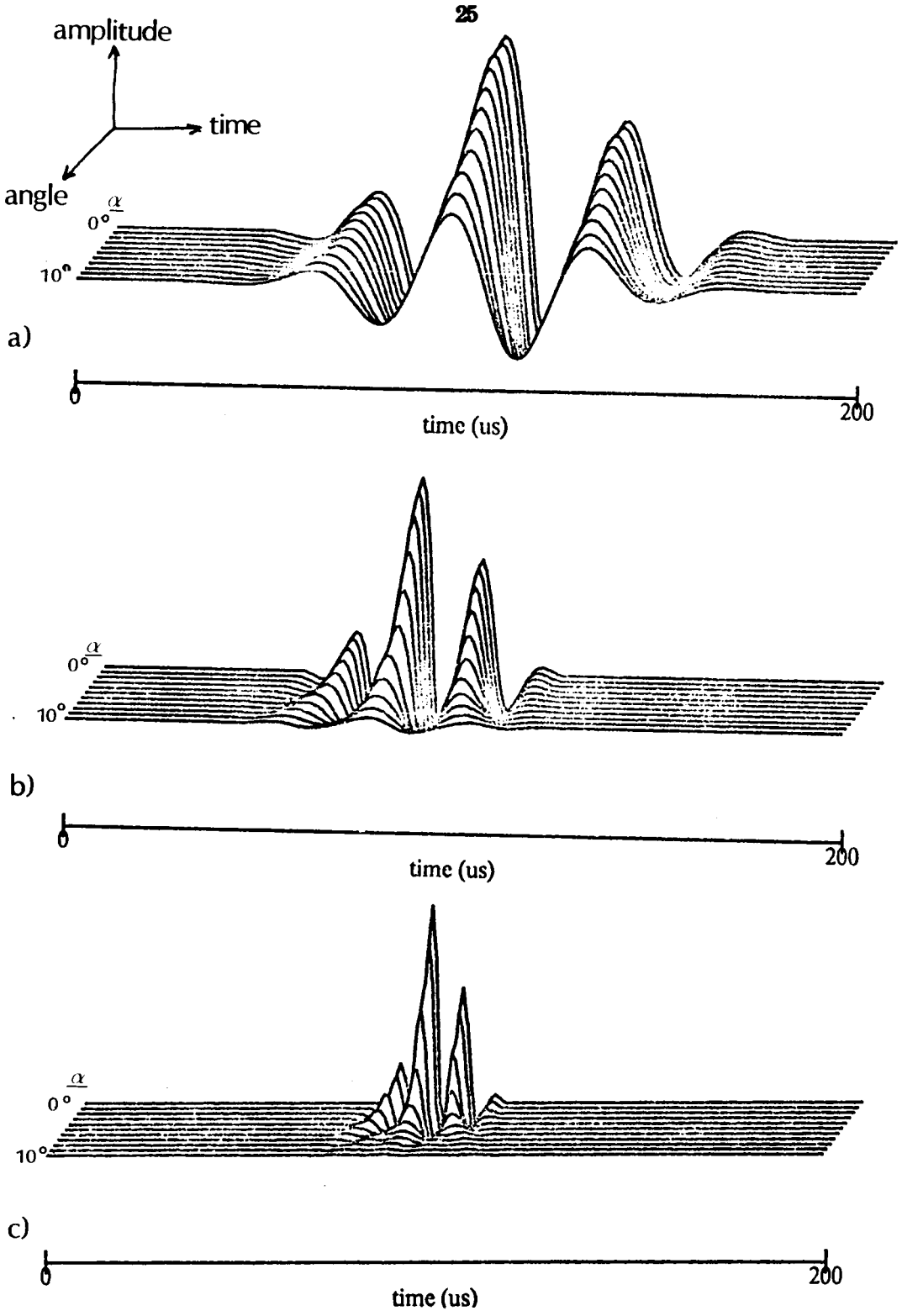

Figure 11: Convolution of pulse waveforms with T/R pair impulse response shown in Figure 7: *a*) 30 KHz, *b*) 60 KHz, *c*) 120 KHz.

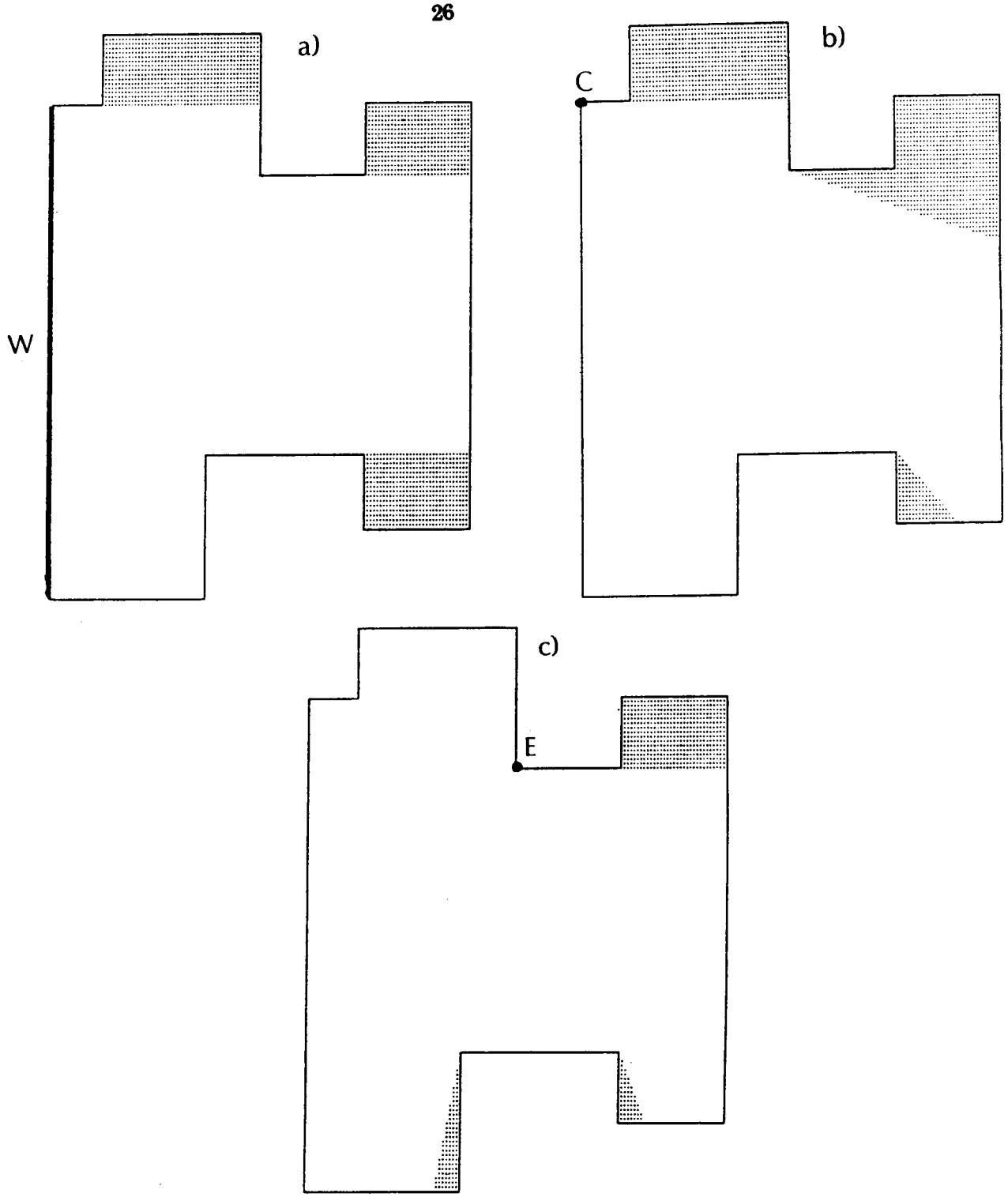

Figure 12: Shadow regions in the floor plan: *a*) Shadows for wall W, *b*) Shadows for corner C, *c*) Shadows for edge E.

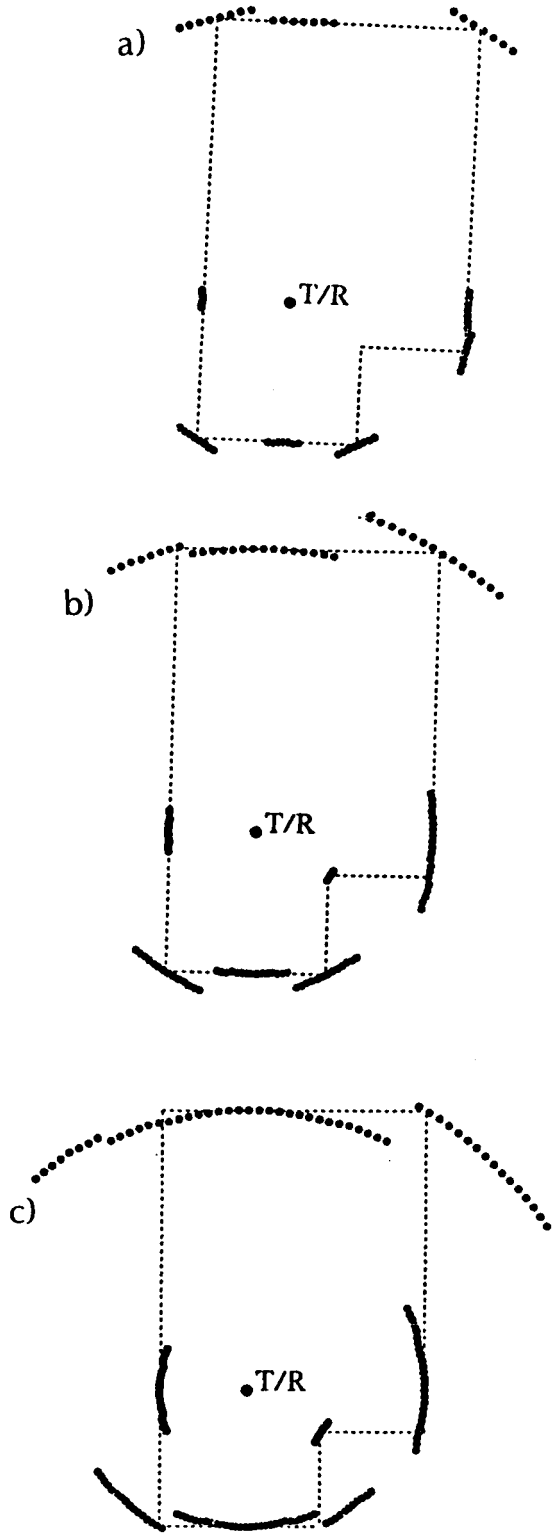

Figure 13: Sector sonar maps of CEW0 using three different threshold settings: *a*) -20 dB, *b*) -40 dB, and *c*) -60 dB (relative to wall reflection). Dot labeled "T/R" indicates transducer location. Dashed lines indicate true floor plan.

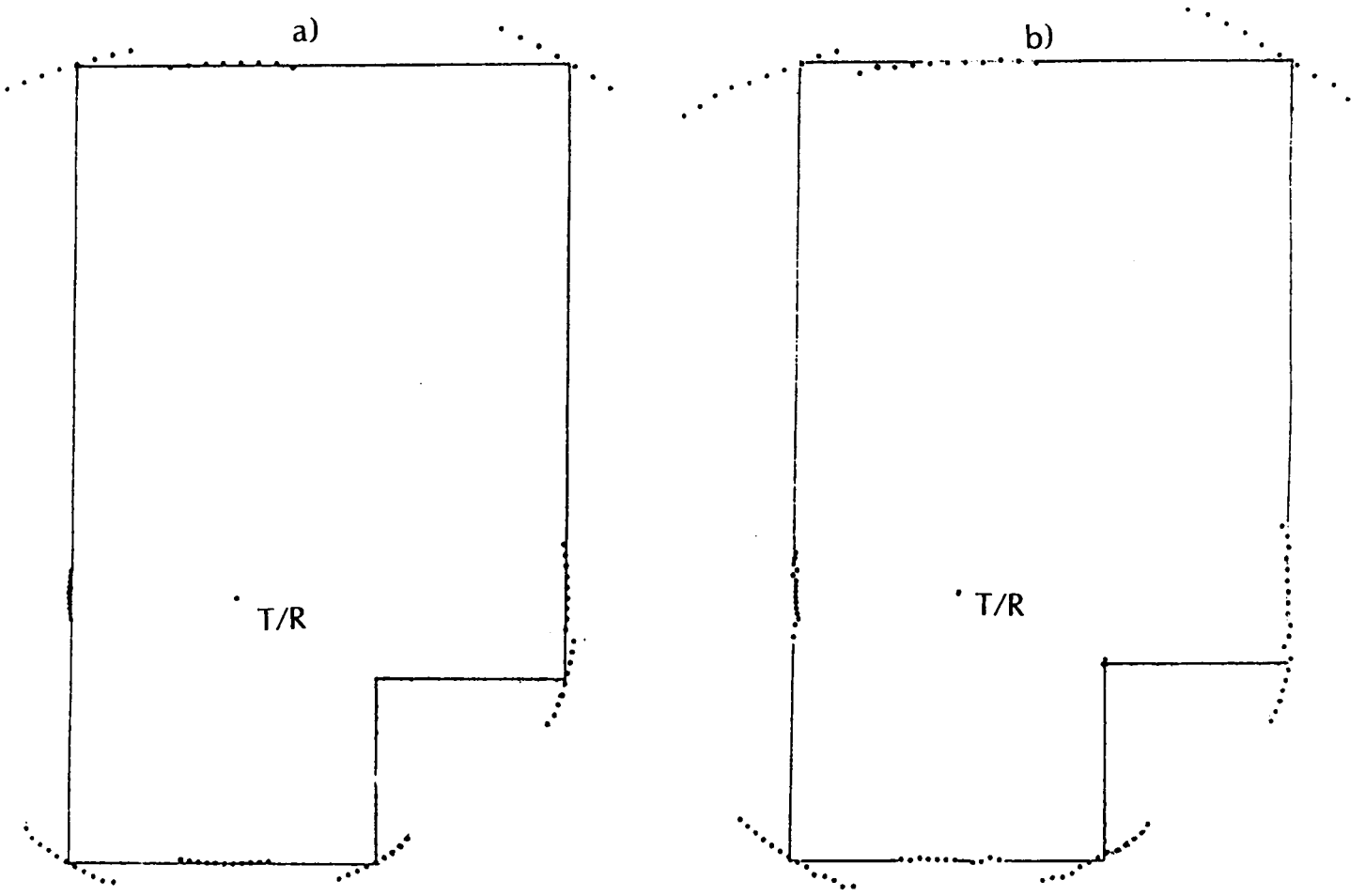

Figure 14: Actual Sector sonar maps obtained with a Polaroid transducer, using different threshold settings:
a) -20 dB, and *b*) -36 dB (relative to wall reflection).
Dot labeled "T/R" indicates transducer location.
Solid lines indicate true floor plan.

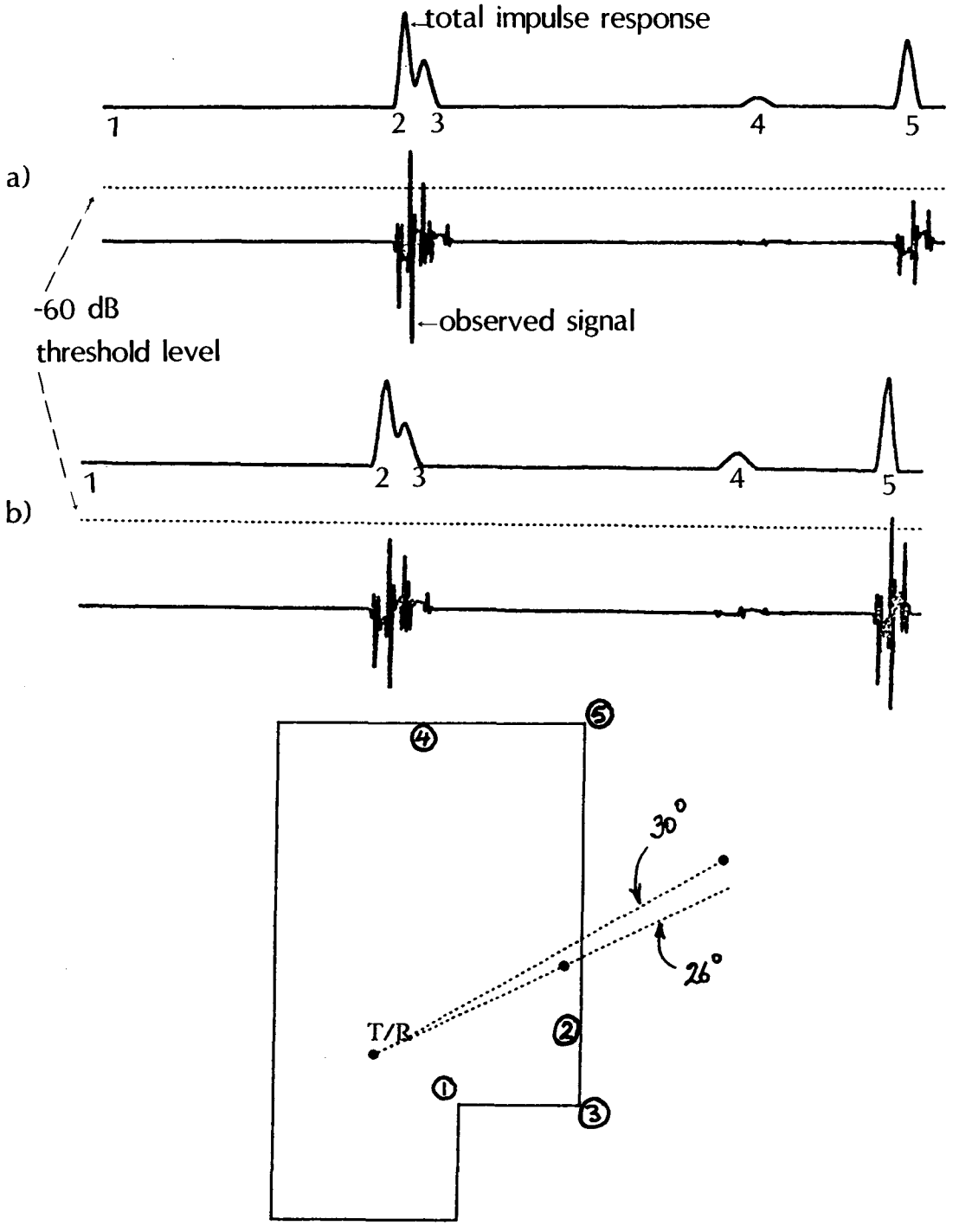

Figure 15: *Explanation for large range jumps in Figure 13c:*
a) Signals observed for transducer azimuth equal to 26°,
b) Signals observed for transducer azimuth equal to 30°.
The time axis starts near the beginning of the impulse response of the closest element. The contributions from the various elements are indicated by the circled numbers.

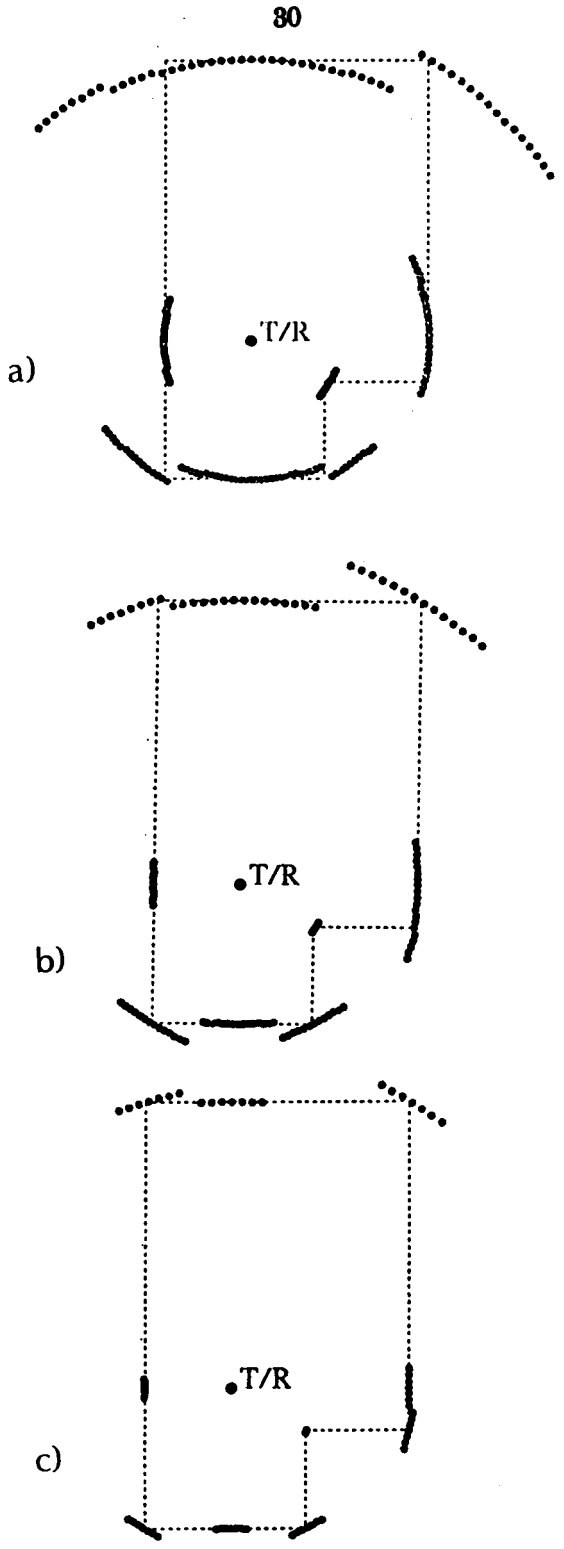

Figure 16: Sector sonar maps of CEW0 using three different resonant frequency transducers: *a*) 30 KHz, *b*) 60 KHz, and *c*) 120 KHz. Threshold -40 dB. Dot labeled "T/R" indicates transducer location. Dashed lines indicate true floor plan.

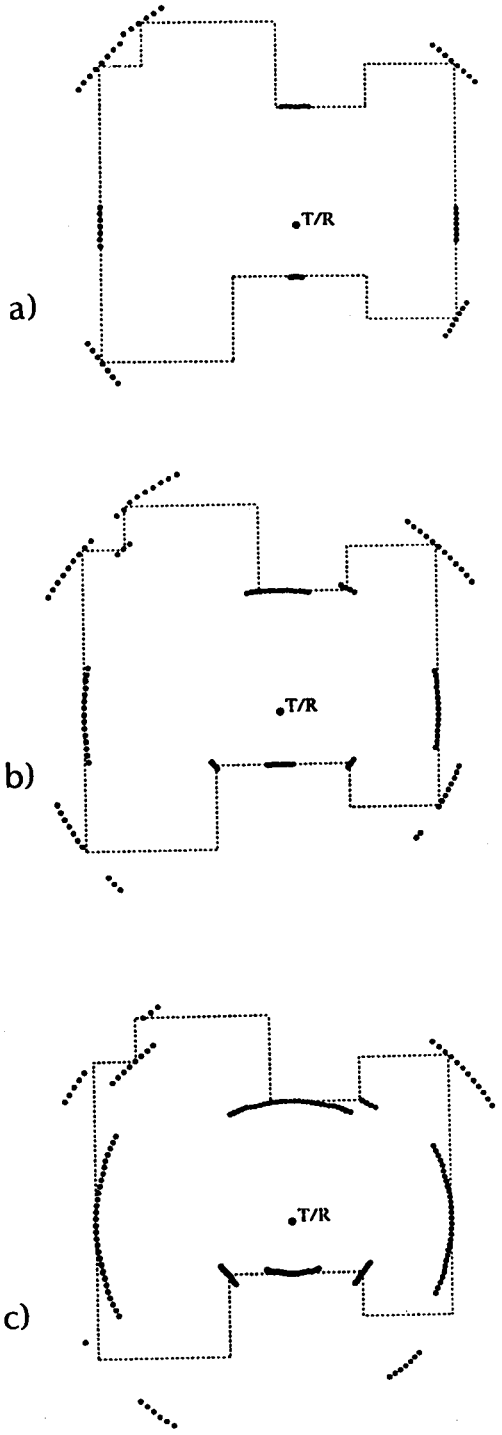

Figure 17: Sector sonar maps of CEW1 using three different threshold settings: *a*) -20 dB, *b*) -40 dB, and *c*) -60 dB (relative to wall reflection). Dot labeled "T/R" indicates transducer location. Dashed lines indicate true floor plan.

References

1. Moravec, H.P. and Elfes A., "High resolution maps from wide angle sonar", *IEEE International Conference on Robotics and Automation*, 1985, pp. 116-121.

2. Crowley, J.L., "Dynamic world modeling for an intelligent mobile robot using a rotationg ultrasonic ranging device", *IEEE International Conference on Robotics and Automation*, 1985, pp. 128-135.

3. Polaroid Corporation, *Ultrasonic Range Finders,* Polaroid Corporation, 1982.

4. Schwarz, R. and Friedland, B., *Linear System Theory,* McGraw-Hill, 1964.

5. Morse, P.M. and Ingard, K.U., *Theoretical Acoustics,* McGraw-Hill, 1968.

6. Oppenheim,A. and Shafer, R., *Digital Signal Processing,* Prentice-Hall, 1975.

7. Wells, P.N.T, *Biomedical Ultrasonics,* Academic Press, 1977.

8. Gradshteyn, I.S. and Ryzhik, I.M., *Table of Intergals, Series and Products,* Academic Press, 1980.

9. Alberto Elfes, "untitled", private communication. Data taken in a relatively uncluttered laboratory room, but previously defying interpretation, have successfully been interpreted using the approach we describe.